How to cite: *Angew. Chem. Int. Ed.* **2024**, *63*, e202405618
doi.org/10.1002/anie.202405618

Electrochemistry

para-Aminoazobenzenes—Bipolar Redox-Active Molecules

*Dominic Schatz, Marcel E. Baumert, Marie C. Kersten, Finn M. Schneider, Mogens Brøndsted Nielsen, Max M. Hansmann, and Hermann A. Wegner**

Abstract: Azobenzenes (ABs) are versatile compounds featured in numerous applications for energy storage systems, such as solar thermal storages or phase change materials. Additionally, the reversible one-electron reduction of these diazenes to the nitrogen-based radical anion has been used in battery applications. Although the oxidation of ABs is normally irreversible, 4,4'-diamino substitution allows a reversible $2e^-$ oxidation, which is attributed to the formation of a stable bis-quinoidal structure. Herein, we present a system that shows a bipolar redox behaviour. In this way, ABs can serve not only as anolytes, but also as catholytes. The resulting redox potentials can be tailored by suitable amine- and ring-substitution. For the first time, the solid-state structure of the oxidized form could be characterized by X-ray diffraction.

Introduction

Since their discovery in 1834 by Mitscherlich, azobenzenes (ABs) have continuously been present in chemical research.[1] The straightforward synthesis of simple ABs, and their bright coloration sparked their application in the dye industry, where still today 70 % of the total dye production is based on these diazenes.[2] The work of Domagk at the IG Farben (German for "Dye industry syndicate stock corporation"), where the antibacterial properties of diazene dyes were studied, was awarded the Nobel Prize in 1939.[3] With the identification of the light-induced isomerization from the stable *E*- to the metastable *Z*-isomer by Hartley, the interest in these compounds has grown even more.[4] In recent years ABs have found their way into photoactivated pharmacology,[5] light induced conformation changes in biological macromolecules[6] or alignments in liquid crystalline phases,[7] as photon-driven molecular machines,[8] as a tool to reversibly change shapes of soft materials,[9] or as a Molecular Wind-up meter.[10] Another important application of ABs are energy storage systems. Here, the parent *E*-isomer is irradiated with light of a specific wavelength, and after photoisomerization, energy is stored in the resulting *Z*-state. This energy can then be released by the backreaction to the *E*-configuration. If the *Z*-isomer has a lower melting point than the *E*-isomer, solid-to-liquid phase transition can occur during the solar energy uptake.[11] This way, thermal energy from the surrounding medium is additionally stored in the phase transition, increasing the energy density of these systems further. So-called molecular solar thermal energy storage systems (MOST) rely on the storage of solar energy in bond strain, and an efficient release of this strain. There are a variety of different methods to release the strain, such as thermal activation,[12] catalysis[13] or, by electron- or hole-catalysis.[14,15] The electron catalysis of the back isomerization proceeds via the formation of a stable radical, which is located on the N–N bond. The sterically encumbered *Z*-isomer is locked in its place due to the rigid nature of the N=N double bond. If a radical is placed on the diazene subunit, the nitrogen loses its double bond character and can rotate unhindered to the *E*-form. The subsequent transfer of the electron from an already isomerized *E*- to another AB in its *Z*-state makes this process catalytic in electrons. Similar to this reductive behavior, a radical produced by the oxidation of AB undergoes the catalytic isomerization in an analogous fashion. The difference between both of these transformations is that the $1e^-$ reduction of AB is a reversible process, which means that no AB is destroyed, as shown in an electron triggered energy release from a thiophene based AB with excellent cyclability.[16]

The reversibility of the reduction of AB has led to yet another application of AB in energy storage: Recently, Zhang et al. used AB as the anolyte in redox-flow batteries (RFB),[17] and soon after a variety of RFB layouts based on AB followed,[18,19] adding to the ever-increasing space of

[*] D. Schatz, M. C. Kersten, F. M. Schneider, Prof. Dr. H. A. Wegner
Institute of Organic Chemistry
Justus Liebig University
Heinrich-Buff-Ring 17, 35392 Gießen (Germany)
E-mail: hermann.a.wegner@org.chemie.uni-giessen.de

D. Schatz, M. C. Kersten, F. M. Schneider, Prof. Dr. H. A. Wegner
Center of Materials Research (ZfM/LaMa)
Justus Liebig University
Heinrich-Buff-Ring 16, 35392 Gießen (Germany)

M. E. Baumert, Prof. Dr. M. M. Hansmann
Faculty of Chemistry and Chemical Biology (CCB)
Technical University of Dortmund
Otto-Hahn Str. 6. 44227 Dortmund (Germany)

Prof. Dr. M. B. Nielsen
Department of Chemistry
University of Copenhagen
2100 Copenhagen (Denmark)

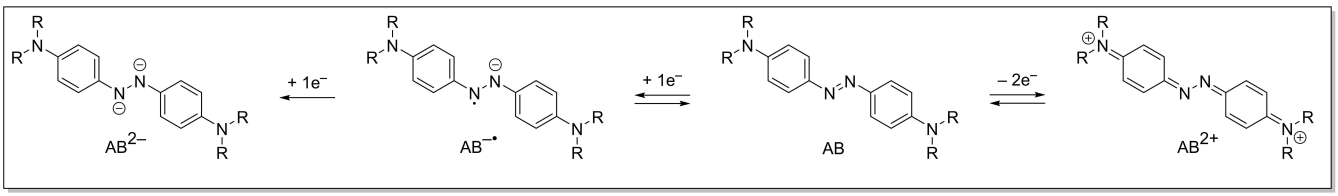

Figure 1. The reversible 1e⁻ reduction of AB to the anion radical AB⁻•, the irreversible 2e⁻ reduction to the dianion AB^{2-}, and the proposed 2e⁻ oxidation to a bis-quinoidal structure AB^{2+}.

organic, redox-active compounds for electrochemical energy storage.[20] These AB-based RFB rely on the redox activity of the N=N azo bond, which can reversibly be reduced to the radical anion in a 1e⁻ process, followed by an (normally) irreversible second 1e⁻ reduction to the dianion. The irreversibility of the second reduction wave was rationalized by the protonation of the rather basic, electron-rich nitrogen in the reduced form.[21] The nature of the stable radical anion has been supported by electron paramagnetic resonance spectroscopy (EPR) of azobenzene-d_{10}, where the resulting 5-line hyperfine structure confirms one electron interacting with two equivalent nitrogen atoms.[22] The product of the second reduction is diamagnetic, and does not show any EPR signal. Cyclic voltammetry of the more electron-poor 4,4'-azopyridine, however, shows reversibility of both 1e⁻ reductions, which is due to the relatively lower basicity in comparison to unsubstituted AB.[23]

Although the 2e⁻ oxidation of AB is normally irreversible, substitution in *ortho*- or *para*-position of each phenyl unit with hydroxyl or amino groups can overcome this obstacle. This change is ascribed to the formation of a stable bis-quinoid structure of the dication upon oxidation (Figure 1). The structure of the oxidation product from 4,4'-diamino AB has not been confirmed yet, although calculations are in agreement with the proposed bis-quinoid structure.[15] Combining the 1e⁻ reduction of the azo bond with the 2e⁻ oxidation to the bis-quinone offers the possibility to employ these compounds as bipolar substrates in symmetrical RFB, where the same compound is used as the anolyte and the catholyte. These symmetrical energy storage systems have advantages over conventional layouts, as they do not suffer from long-term capacity decay by transportation of active materials through the separating membrane.[24] In fact, reversal of the cell's polarity after a specific amount of cycles can effectively double the battery's lifetime. Here, the imbalance of the redox equivalents of the oxidation or reduction respectively could increase the lifetime by polarity reversal further.

As the redox behavior is highly dependent on the solvent used as well as the electrolyte, we investigated various conditions to ensure reversibility of the oxidation and the reduction. Furthermore, we evaluated the effects of changes in the chemical structure of the aromatic ring, as well as the *para*-amino group to elucidate structure–property relationships as well as to optimize the compounds for electrochemical applications. To get more insight into the structure of the oxidized form, its molecular structure was characterized by single crystal X-ray diffraction. This is, to the best of our knowledge, the first confirmation of a quinoidal AB structure obtained from oxidation. The insights into the redox properties will broaden the use of the AB scaffold in energy storage systems, expanding the already versatile profile of diazene compounds.

Results and Discussion

The 4,4'-bisamino AB motif offers two possibilities to diversify its chemical structure and to study the resulting structure-redox-properties relationship: substitution pattern on the aromatic rings, and varying substituents at the amines (Scheme 1). In this study, both possible positions (2,2'- and 3,3'-) of a symmetrical bis-substituted AB were substituted with electron-withdrawing fluorine- or electron-donating methoxy groups. Starting from either commercially available or readily synthesizable 4-bromoanilines **1a–d**,[25] 4,4'-dibromo-ABs **2a–d** were prepared in good yields by oxidation with activated MnO_2. The 4,4'-dibromo AB without additional substituents was prepared by copper catalyzed aerobic coupling of 4-bromoaniline **1e** in good yields.[26] The *para*-Br substituent conveniently allows to introduce the amino group via palladium catalyzed Buchwald–Hartwig coupling reaction.[27] For the ring-substituted AB **3a–d**, diethylamine was employed as the coupling partner of choice. The utilization of diethylamine instead of dimethylamine is due to its better solubility as well as easier and safer handling (liquid vs. gas). The electron-rich methoxy derivatives **3a–b** were isolated after column chromatography in moderate yields, while the yield of the fluorine derivatives **3c–d** was generally lower. We found evidence of products resulting from nucleophilic aromatic

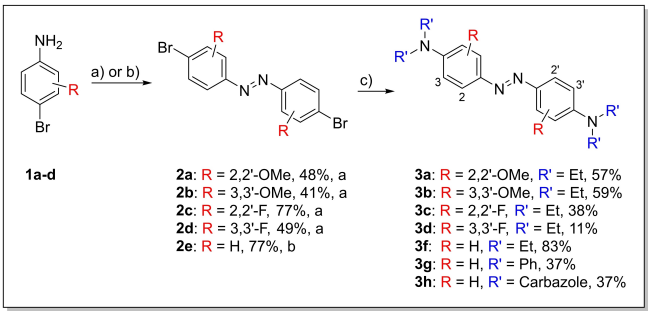

Scheme 1. Preparation of symmetric redox-active AB structures **3a–h**. a) Activated MnO_2, toluene, 70 °C, 24 h to 48 h. b) CuBr, pyridine, toluene, 60 °C, under air, 24 h. c) HNR'_2, $Pd_2(dba)_3$, RuPhos, Cs_2CO_3, toluene, 100 °C, 24 h to 72 h.

substitution of similar electron-poor ABs (see Supporting Information Figure S28), which results in more tedious purification and lower yields. Diversification of the amine functionality was achieved by Buchwald–Hartwig coupling of the 4,4'-dibromo compound **2e** with varying amine partners. Two aryl (**3g–h**) and one alkyl amine (**3f**) were synthesized in this fashion, while the dimethyl derivative **3e** was synthesized by CuBr coupling of the corresponding aniline (see Supporting Information page 18).[26]

The solvent and the electrolyte are crucial for a successful electrochemical experiment. Different combinations of both were screened. The diethyl derivative **3f** was employed as the model compound in a 2 mM concentration, with 1 mM decamethylferrocene (Fc*) as an internal standard.

Propylene carbonate (PC), dichloromethane (DCM) and acetonitrile (ACN) were tested as solvents with 0.2 M tetra-*n*-butylammonium hexafluorophosphate ($TBAPF_6$) as electrolyte (Figure 2). For the green solvent PC, AB **3f** showed only limited solubility, as well as an irreversible reduction. Deprotonated pyridazinones are known to irreversibly open propylene carbonates, and a similar nucleophilic attack could occur with the very electron-rich radical anion, resulting in the irreversible reduction.[28] In the case of DCM, no reversible reduction was observed. On the other hand, the expected $2e^-$ oxidation peak was split into two fully reversible $1e^-$ oxidations, indicating the formation of a stable mono-cation radical. This is in accordance with titration experiments, that showed that the chemical oxidation of 4,4'-diamino AB does indeed proceed via a radical cation, and both oxidation peaks are electrochemically very close.[15] DCM was the only solvent we tested that allowed a differentiation of both $1e^-$ oxidations at slow scanning rates. Interestingly, when ACN was used as a solvent, the reduction process became more evident, but still irreversible. This is surprising, as unsubstituted AB in ACN with $TBAPF_6$ has already been employed in an asymmetric battery setup and showed good cyclability.[18] To examine the effect of electrolytes, *N*,*N*-dimethylformamide (DMF) was employed as the reference solvent. With lithium bis(trifluoromethanesulfonyl)imide (LiTFSI), the oxidation stays reversible but the reduction is irreversible. Additionally, a second oxidation peak appears that may be referenced to the initial irreversible reduction, as this peak is not present if only the oxidation is scanned (see Supporting Information Figure S5). This large peak-to-peak separation could be due to the high affinity of Li^+ cations with the $N{=}N^-$ motif that forms upon reduction.[17] This effect might be increased due to the electron rich motif of the 4,4'-diamino AB versus unsubstituted AB. Comparing the voltage profiles of tetra-*n*-butylammonium tetrafluoroborate ($TBABF_4$) and $TBAPF_6$ solutions highlights the important role of the electrolyte cation. While the PF_6^- salt shows good reversibility for the $2e^-$ oxidation, as well as for the $1e^-$ reduction of the parent compound, a low current flow was observed for the boron equivalent. One reason for that could be the deposition of insoluble BF_4^- salts on the electrode (see below), as shown by successively scanning (see Supporting Information Figure S7). Nevertheless, the DMF/$TBAPF_6$ electrolyte system allows to reversibly access three different redox states of our AB: neutral AB, the reduced radical anion, and the oxidized bis-quinoidal dication structure.

To optimize the redox activity of 4,4'-amino ABs, the influence of the amino groups was investigated (Figure 3, bottom). With the elongation of the alkyl group from methyl (**3e**) to ethyl (**3f**), no significant change of the peak potentials or the voltage window was observed, although the solubility of the ethyl derivative **3f** was superior to **3e** (32 mg/mL and 2.1 mg/mL for **3f** and **3e** in DMF, respectively). Changing the substituents from alkyl to an aromatic phenyl group (**3g**) facilitated the reduction by 400 mV, and shifted the oxidation by +300 mV. This might be explained by the more electron poor amine, leading ultimately to a lower electron density in the AB core. When the nitrogen atom was incorporated into the aromatic carbazole motif (**3h**), the redox behavior changes drastically. Compound **3h** is reduced at −1.10 V and oxidized at 1.47 V, but both of these reactions proceed irreversibly. As carbazole itself can show irreversible redox processes with complex reaction

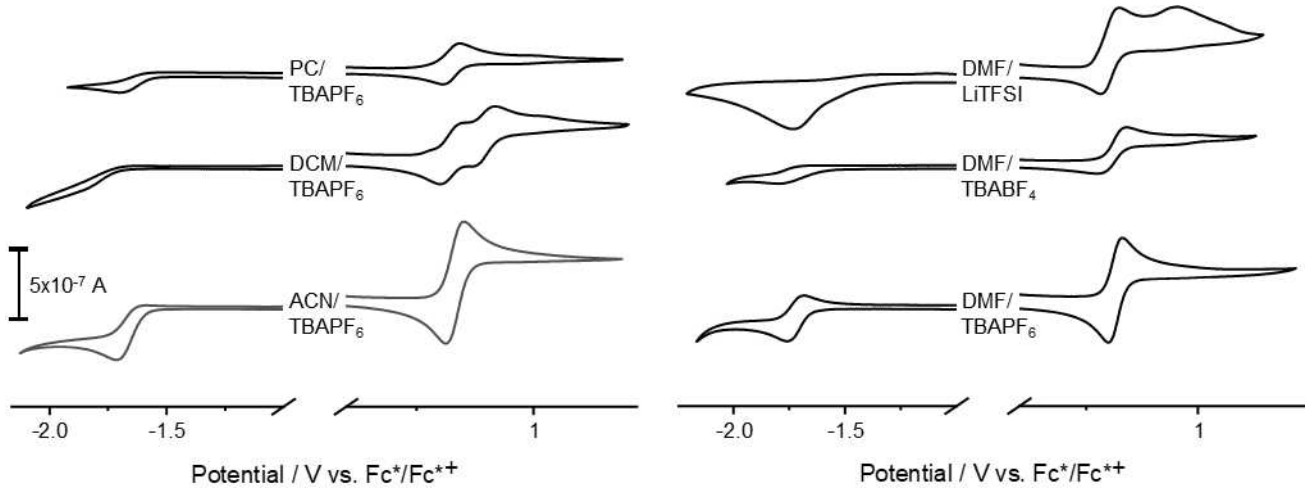

Figure 2. Cyclic voltammograms of model compound **3f** with varying conductive salts and organic solvents. Solutions were prepared with 2 mM of **3f**, 200 mM salt and 1 mM Fc* as an internal standard. Potentials are referenced to the standard and measured with a scan rate of 100 mV/s.

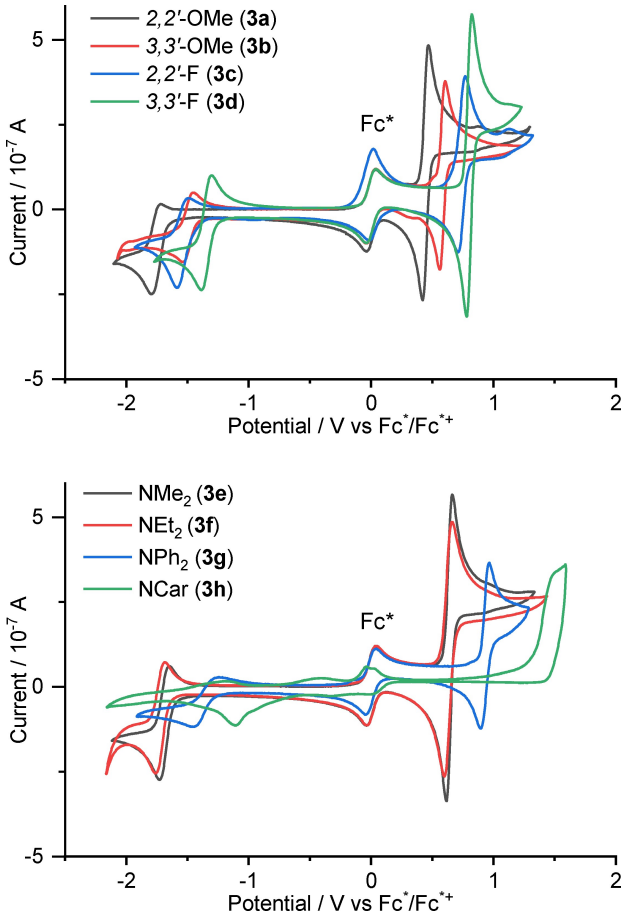

Figure 3. Influence of substitution of the 4,4'-amino AB scaffold in the cyclic voltammograms of compounds **3a–h** in DMF/TBAPF$_6$ electrolyte measured with a scan rate of 100 mV/s. Measured with and referenced to Fc*.

Table 1: Peak potentials of substituted ABs **3a–h** in DMF/TBAPF$_6$ at 100 mV/s vs Fc*.

Substitution Pattern	E_{red} /V	E_{ox} /V	$\Delta E_{ox\text{-}red}$ /V
2,2'-OMe (**3a**)	−1.74	0.62	2.36
3,3'-OMe (**3b**)	−1.49	0.59	2.08
2,2'-F (**3c**)	−1.54	0.72	2.26
3,3'-F (**3d**)	−1.34	0.80	2.14
NMe_2 (**3e**)	−1.68	0.64	2.32
NEt_2 (**3f**)	−1.73	0.63	2.36
NPh_2 (**3g**)[a]	−1.33	0.94	2.27
NCar (**3h**)[b]	−1.10	1.47	2.57

[a] Due to low solubility, only 1 mM concentration of substrate.
[b] Irreversible redox behavior.

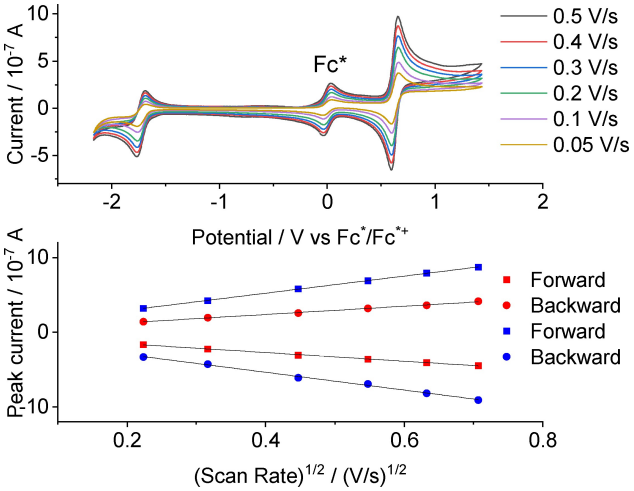

Figure 4. Electrochemical characterization of **3f**. Top: Cyclic voltammogram of **3f** in 2 mM concentration with 200 mM TBAPF$_6$ conducting salts at different scan rates from 0.5 V/s to 0.05 V/s. Bottom: Plot of the reduction and re-oxidant (red) and of the oxidation and re-reduction (blue) peak currents versus the square root of the scan rate.

products, the combination with AB might show a similar behavior.[29]

Additionally, electron-withdrawing fluorine and electron-donating methoxy groups were placed in the *ortho*- or *meta*-position of the AB core (Figure 3, top). Here, the most important observation is the decrease in the reversibility of *ortho*-substituted derivatives **3a** and **3c**. Redox peak positions can be fine-tuned by adding these groups, but the voltage window between reduction and oxidation is not larger in comparison to the unsubstituted analogs, ultimately not resulting in an improved electrochemical storage potential (Table 1).

For the diethyl derivative **3f**, which shows the largest ΔE of the tested substrates, good reversibility can be demonstrated on the CV timescale (Figure 4 top). A linear relationship between the peak currents and the square root of the scan rate reveals a diffusion-controlled behavior for the reduction, as well as for the oxidation (Figure 4 bottom). Diffusion coefficients for **3f** obtained from the Randles–Sevcik equation give different values depending on which forward redox process is monitored, with 1.36×10^{-6} cm^{2}s^{-1} and 8.29×10^{-7} cm^{2}s^{-1} for reduction and oxidation respectively. These values are comparable to other organic materials,[30] and to unsubstituted AB.[17] Diffusion coefficients of the back reactions gave 1.01×10^{-6} cm^{2}s^{-1} for the radical anion and 8.73×10^{-6} cm^{2}s^{-1} for oxidized species **3f^{2+}**. Even at high concentrations of 100 mM or at saturation, reversibility is observed (SI Figures S9 and S10). According to these cyclic voltammetry studies, the bis-*para*-alkylamine substituted AB offers the possibility to be employed in symmetrical RFB as a bipolar, redox-active material.

To further explore their electrochemical properties, charge/discharge studies in an H-cell were performed. As the application of AB as the anolyte is well established, we employed compound **3f** as the catholyte (see Supporting Information page 42). AB **3f^{2+}** was electrochemically synthesized and then cycled in a symmetrical H-cell with neutral compound (**3f**/**3f^{2+}**) under galvanostatic charge/discharge (2 C) in DMF (see Supporting Information Figure S22 and S23). Under these conditions a capacity decay of approximately 30 % was observed after 10 cycles. Additionally, the charging was performed with the chemically oxidized **3f^{2+}** in a symmetrical H-cell utilizing ACN as the solvent, which

slightly increased the performance (approximately 25 % decay after 10 cycles, see Supporting Information Figure S24 and S25). Unfortunately, we were not able to cycle the $1e^-$ reduction in DMF, most probably due to the high basicity of our employed AB **3f**, leading to instability over the time-frame of our cycling experiments.

The reduction of AB has been studied thoroughly, and the $1e^-$ reduced species has been identified as the radical anion, while the $2e^-$ species corresponds to the double deprotonated hydrazine. For the oxidation of 4,4'-disubstituted AB with amines or with hydroxides, the bis-quinoidal structure is the assumed species. The formation of the stable quinone structure by bis-*para*-substitution is thought to be responsible for the fully reversible oxidation. Albeit the occurrence of the quinoidal structure is observed for "Weitz type" 4,4'-bispyridinium salts,[31] and theoretical calculation support the presence of a similar bonding type in ABs,[15] to the best of our knowledge, no experimental characterization is available. By using the chemical oxidant $NOBF_4$ in ACN solution, removing the solvent and vapor diffusion of diethyl ether from DCM, crystals suitable for X-ray diffraction were obtained. The double positively charged AB crystallized with two BF_4^- anions and one H_2O molecule in the $P_{21/n}$ space group. The low solubility of the crystallized product might explain the irreversible behavior in electrolyte solution containing a BF_4^- counter ion. The needle-like crystals appear blue or orange, depending on the viewing angle. By comparing it with the parent AB, an increase of the N_{azo}–N_{azo} bond length (1.27 to 1.36 Å), as well as a decrease of the N_{azo}–C_{aryl} bond length from 1.42 to 1.32 Å was observed (Figure 5).[32] These lengths are consistent with density functional theory (DFT) calculations.[15]

Additionally, there is a bond length alternation of C_{aryl}–C_{aryl} in the ring system. From the bond lengths c, d, e, c', d', and e', the quinoid characters[34] of $\delta_r = 0.019$ Å and 0.100 Å are obtained for **3f** and $\mathbf{3f^{2+}}$, respectively. The large value of 0.100 Å supports the fully quinoid structure of the oxidized form. To verify that the oxidized species formed by chemical oxidation equals the one formed during electrochemical analysis, **3f** was titrated with $NOBF_4$ (1.0–2.0 eq.) and the change in absorbance was analyzed. The obtained spectra were compared to measurements in a spectroelectrochemistry cell (Figure 6 and Supporting Information page 40).

The experiments show the decrease of the neutral AB **3f** π–π* band at around 470 nm, and an increase of a band at around 380 nm of $\mathbf{3f^{2+}}$. Both spectral changes pass over a species at 680 nm, which was assigned to a radical cation in previous studies.[15] This supports that the fully quinoidal structure obtained by chemical oxidation is the same as that observed during electrochemical measurements.

Conclusion

We presented the application of 4,4'-diamino ABs as bipolar redox-active materials. The combination of DMF and $TBAPF_6$ as an electrolyte allows $1e^-$ reduction of the N=N bond, as well as the stable formation of a bis-quinoidal form by a $2e^-$ oxidation process. We employed our model substrate as a redox couple $\mathbf{3f/3f^{2+}}$ in symmetric H-cell cycling experiments and observed a notable capacity decay over multiple cycles. Here, additional molecular engineering is needed to allow for a fully operational symmetrical RFB. One approach could be the shielding of the resulting Michael system. Making the whole AB less electron-rich might facilitate the $1e^-$ reduction for cycling experiments. The formation of this oxidized form in the hitherto only predicted oxidation mechanism was further elucidated by X-ray analysis, which strongly suggests the presence of an azobenzene-quinoidal structure. By attaching electron donating or withdrawing substituents, the potentials can be fine-tuned, ranging from −1.34 to −1.74 V for the reduction,

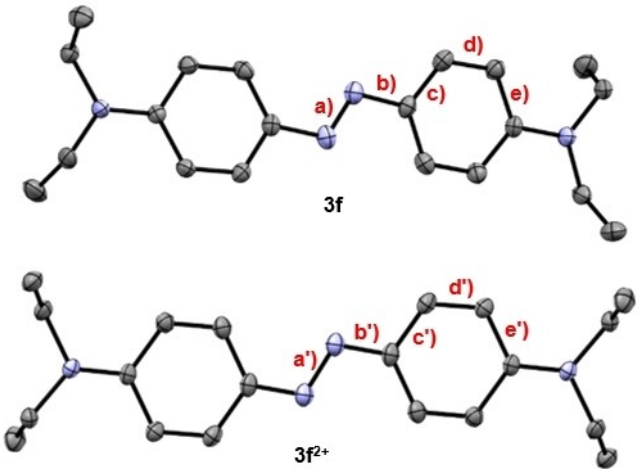

Figure 5. Solid-state structures of AB **3f** (from CCDC: 1000644)[32] and $\mathbf{3f^{2+}}$ (CCDC: 2247535) from the chemical oxidation with $NOBF_4$. Solvent molecules, hydrogens and counter anions are omitted for clarity. Thermal ellipsoids are shown at 50% probability. Bond lengths in Å: *a* = 1.266, a' = 1.363, *b* = 1.423, b' = 1.321, *c* = 1.385, c' = 1.442, d = 1.382, d' = 1.346, e = 1.417, e' = 1.450.[33]

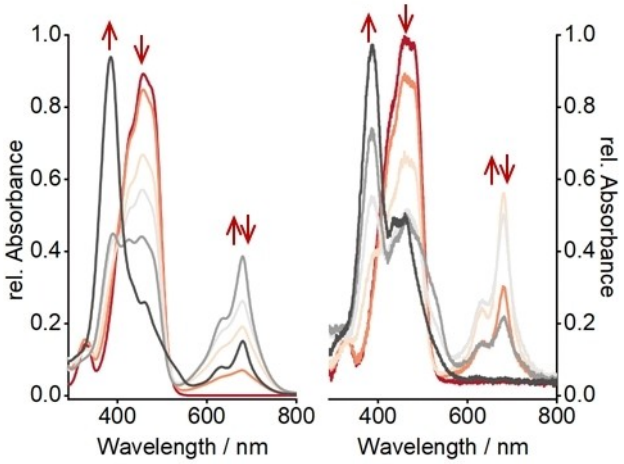

Figure 6. UV/Vis absorption spectra (left) of **3f** in ACN titrated with chemical oxidant $NOBF_4$, and spectra resulting from spectroelectrochemical analysis (right) of **3f** in ACN. Increasing oxidation from red to black.

and 0.59 to 0.80 V for the oxidation. Aryl substituents seem to influence the redox behavior the most, but show inferior redox properties, due to their irreversibility and low solubility. Elongation of alkyl substituents at the amine-nitrogen improves solubility, while retaining the redox behavior. These results provide the essential basis for application of AB derivatives in the important field of (electrochemical) energy storage.

Acknowledgements

The authors thank BMEL (Federal Ministry of Food and Agriculture) within the project FOREST (62000958) and DFG (HA-8832/2-1) for funding, Prof. Peter R. Schreiner for providing the electrochemical cell setup. Open Access funding enabled and organized by Projekt DEAL.

Conflict of Interest

The authors declare no conflict of interest.

Data Availability Statement

The data that support the findings of this study are available in the supplementary material of this article.

Keywords: azo compounds · electrochemistry · cyclic voltammetry · energy conversion · redox chemistry

[1] E. Mitscherlich, *Ann. Pharm.* **1834**, *12*, 311–314.
[2] F. A. Jerca, V. V. Jerca, R. Hoogenboom, *Nat. Chem. Rev.* **2022**, *6*, 51–69.
[3] Elsevier Publishing Company (Hrsg.) *Lex Prix Nobel*, Amsterdam, **1965**.
[4] G. S. Hartley, *Nature* **1937**, *140*, 281.
[5] a) M. M. Lerch, M. J. Hansen, G. M. van Dam, W. Szymanski, B. L. Feringa, *Angew. Chem. Int. Ed.* **2016**, *55*, 10978–10999; b) J. Broichhagen, J. A. Frank, D. Trauner, *Acc. Chem. Res.* **2015**, *48*, 1947–1960.
[6] O. Bozovic, B. Jankovic, P. Hamm, *Nat. Chem. Rev.* **2022**, *6*, 112–124.
[7] T. I. Y. Yu, *J. Photochem. Photobiol. C* **2004**, *5*, 247–265.
[8] W. R. Browne, B. L. Feringa, *Nat. Nanotechnol.* **2006**, *1*, 25–35.
[9] X. Pang, J. -Lv, C. Zhu, L. Qin, Y. Yu, *Adv. Mater.* **2019**, *31*, e1904224.
[10] C. Averdunk, K. Hanke, D. Schatz, H. A. Wegner, *Acc. Chem. Res.* **2024**, *57*, 257–266.
[11] B. Zhang, Y. Feng, W. Feng, *Nano-Micro Lett.* **2022**, *14*, 138.
[12] T. J. Kucharski, N. Ferralis, A. M. Kolpak, J. O. Zheng, D. G. Nocera, J. C. Grossman, *Nat. Chem.* **2014**, *6*, 441–447.
[13] D. Schulte-Frohlinde, *Liebigs Ann.* **1958**, *612*, 131–138.
[14] A. Goulet-Hanssens, M. Utecht, D. Mutruc, E. Titov, J. Schwarz, L. Grubert, D. Bléger, P. Saalfrank, S. Hecht, *J. Am. Chem. Soc.* **2017**, *139*, 335–341.
[15] A. Goulet-Hanssens, C. Rietze, E. Titov, L. Abdullahu, L. Grubert, P. Saalfrank, S. Hecht, *Chem* **2018**, *4*, 1740–1755.
[16] E. Franz, A. Kunz, N. Oberhof, A. H. Heindl, M. Bertram, L. Fusek, N. Taccardi, P. Wasserscheid, A. Dreuw, H. A. Wegner, O. Brummel, J. Libuda, *ChemSusChem* **2022**, *15*, e202200958.
[17] L. Zhang, Y. Qian, R. Feng, Y. Ding, X. Zu, C. Zhang, X. Guo, W. Wang, G. Yu, *Nat. Commun.* **2020**, *11*, 3843.
[18] X. Wang, J. Chai, A. Lashgari, J. J. Jiang, *ChemElectroChem* **2021**, *8*, 83–89.
[19] a) D. Xu, C. Zhang, Y. Zhen, Y. Zhao, Y. Li, *J. Power Sources* **2021**, *495*, 229819; b) X. Zu, L. Zhang, Y. Qian, C. Zhang, G. Yu, *Angew. Chem. Int. Ed.* **2020**, *59*, 22163–22170.
[20] a) J. Winsberg, T. Hagemann, T. Janoschka, M. D. Hager, U. S. Schubert, *Angew. Chem. Int. Ed.* **2017**, *56*, 686–711; b) P. Leung, A. A. Shah, L. Sanz, C. Flox, J. R. Morante, Q. Xu, M. R. Mohamed, C. Ponce de León, F. C. Walsh, *J. Power Sources* **2017**, *360*, 243–283; c) X. Wei, W. Pan, W. Duan, A. Hollas, Z. Yang, B. Li, Z. Nie, J. Liu, D. Reed, W. Wang, V. Sprenkle, *ACS Energy Lett.* **2017**, *2*, 2187–2204; d) V. Singh, S. Kim, J. Kang, H. R. Byon, *Nano Res.* **2019**, *12*, 1988–2001; e) J. Luo, B. Hu, M. Hu, Y. Zhao, T. L. Liu, *ACS Energy Lett.* **2019**, *4*, 2220–2240; f) D. G. Kwabi, Y. Ji, M. J. Aziz, *Chem. Rev.* **2020**, *120*, 6467–6489.
[21] J. L. Sadler, A. J. Bard, *J. Am. Chem. Soc.* **1967**, *90*, 1979–1989.
[22] G. H. Aylward, J. L. Garnett, J. H. Sharp, *Anal. Chem.* **1967**, *39*, 457–460.
[23] A. J. Bellamy, I. S. MacKirdy, C. E. Niven, *J. Chem. Soc. Perkin Trans. 2* **1983**, 183–185.
[24] a) M. L. Perry, J. D. Saraidaridis, R. M. Darling, *Curr. Opin. Electrochem.* **2020**, *21*, 311–318; b) M. Li, J. Case, S. D. Minteer, *ChemElectroChem* **2021**, *8*, 1215–1232; c) R. A. Potash, J. R. McKone, S. Conte, H. D. Abruña, *J. Electrochem. Soc.* **2016**, *163*, A338–A344.
[25] a) Q. Zhou, T. A. Reekie, R. H. Abbassi, D. Indurthi Venkata, J. S. Font, R. M. Ryan, L. Munoz, M. Kassiou, *Bioorg. Med. Chem.* **2018**, *26*, 5852–5869; b) M. Kohn, *J. Org. Chem.* **1953**, *18*, 530–533.
[26] C. Zhang, N. Jiao, *Angew. Chem. Int. Ed.* **2010**, *49*, 6174–6177.
[27] a) S. Samanta, A. Babalhavaeji, M. Dong, G. A. Woolley, *Angew. Chem. Int. Ed.* **2013**, *52*, 14127–14130; b) D. Wu, M. Dong, C. V. Collins, A. Babalhavaeji, G. A. Woolley, *Adv. Opt. Mater.* **2016**, *4*, 1402–1409.
[28] A. Czompa, B. L. Pásztor, J. A. Sahar, Z. Mucsi, D. Bogdán, K. Ludányi, Z. Varga, I. M. Mándity, *RSC Adv.* **2019**, *9*, 37818–37824.
[29] K. Karon, M. Lapkowski, *J. Solid State Electrochem.* **2015**, *19*, 2601–2610.
[30] Y. Yan, S. G. Robinson, M. S. Sigman, M. S. Sanford, *J. Am. Chem. Soc.* **2019**, *141*, 15301–15306.
[31] Z. Liu, M. Frasconi, W.-G. Liu, Y. Zhang, S. M. Dyar, D. Shen, A. A. Sarjeant, W. A. Goddard III, M. R. Wasielwski, J. F. Stoddart, *J. Am. Chem. Soc.* **2018**, *140*, 9387–9391.
[32] K. Gajda, B. Zarychta, Z. Daszkiewicz, A. A. Domanski, K. Ejsmont, *Acta Crys. C* **2014**, *70*, 575–579.
[33] Deposition numbers 2247535 (for **3f**$^{2+}$), 2247536 (Side product of the Buchwald–Hartwig coupling of electron poor azobenzenes, see Supporting Information Figure S28), and 2247537 (for **3h**) contains the supplementary crystallographic data for this paper. These data are provided free of charge by the joint Cambridge Crystallographic Data Centre and Fachinformationszentrum Karlsruhe Access Structures service. These data can be obtained free of charge via https://www.ccdc.cam.ac.uk/structures/.
[34] C. Dehu, F. Meyers, J. L. Brédas, *J. Am. Chem. Soc.* **1993**, *115*, 6198–6206.

Manuscript received: March 22, 2024
Accepted manuscript online: June 13, 2024
Version of record online: July 29, 2024